**Internship Report**
Second Year - Engineering Cycle
**Program :** Autonomous Robotics


Presented by : **Rami Diab**

Supervised by : **Alexis Lefevre**

University : **ENSTA Bretagne**

Host University : **ENSMM / FEMTO-ST**


October 24, 2025

# Contents

# List of Figures

# Abstract

This report presents the work carried out during my internship at the FEMTO-ST laboratory, AS2M department, in Besançon, under the supervision of Dr. Alexis Lefèvre. The project focused on studying the interaction between dielectric particles and non-uniform electric fields to understand and control their motion through dielectrophoresis (DEP). The ultimate objective was to establish a modeling framework capable of describing, and a controller allowing trajectory control of, the movement of a cell in such conditions.

A port-Hamiltonian formalism was developed to represent the system, leveraging its energy-based structure to couple mechanical states (position, momentum) with electrical states (induced polarization and field effects). Several theoretical studies were conducted, including the derivation of dielectrophoretic forces from Maxwell's equations, the use of the Clausius–Mossotti factor to capture material-dependent polarization, and the role of electrode configurations in shaping non-uniform fields. Simulation studies explored field distributions, induced forces, and particle trajectories, providing a deeper understanding of the physics at play and highlighting the potential of the port-Hamiltonian framework for DEP modeling. Numerical simulations were then used to investigate the effect of electrode arrangements and to evaluate the model's ability to reproduce realistic particle dynamics. Finally, a PCB was manufactured to finalize an experimental setup, allowing comparison between the model and experimental data. The first experiments were then conducted to validate the system, providing a first validation of the proposed approach and paving the way for further refinements.

# Introduction

This internship was carried out at the FEMTO-ST Institute, within the AS2M department in Besançon, under the supervision of Dr. Alexis Lefèvre. It took place as part of the second year of the engineering cycle at ENSTA Bretagne, in the Autonomous Robotics program. The project was motivated by the increasing need for advanced methods to model, simulate, and control the behavior of micro- and nano-particles, particularly in biomedical engineering and microfluidics. The ability to manipulate cells or dielectric particles in a precise and reliable way is a key challenge for applications such as targeted drug delivery, lab-on-chip devices, and diagnostic tools.

Among existing techniques, dielectrophoresis (DEP) provides a non-invasive method of control. It relies on the interaction between a dielectric particle and a non-uniform electric field, inducing polarization forces that cause the particle to move. DEP is attractive because it requires only electric actuation, avoiding direct mechanical contact. However, a fundamental difficulty lies in predicting and controlling the motion of particles in such complex environments. For this reason, advanced modeling approaches are required to capture both the physical principles and the energy-based interactions at play.

In this context, the Port-Hamiltonian (pH) framework offers a powerful tool. Port-Hamiltonian systems describe dynamics based on an underlying energy function and a structured interconnection matrix, ensuring that conservation laws and passivity are preserved. Applying this framework to dielectrophoresis enables the modeling of particles and fields in terms of energy storage, dissipation, and exchange with the environment. This provides not only a physically consistent description of the phenomenon, but also a natural basis for designing control strategies that exploit the system's energetic structure. In particular, the pH approach allows the coupling between the electric field and the mechanical motion of a particle to be rigorously expressed, highlighting how electrode voltages can serve as control inputs that shape trajectories.

The internship was structured around two complementary aspects. First, a theoretical and numerical study was conducted, combining the physical principles of DEP with the Port-Hamiltonian formalism. Simulations were carried out to compute electric potentials, fields, and the resulting forces, with the aim of analyzing how electrode configurations influence particle behavior. Second, an experimental platform was developed. A custom printed circuit board (PCB) with micro-electrodes was designed, fabricated, and tested using an oscilloscope to validate signal generation. The platform was then used to perform experiments observing particle motion under DEP forces, providing direct insight into the phenomenon and serving as a first validation step of the theoretical models.

Overall, the internship provided the opportunity to bridge theoretical modeling, based on the Port-Hamiltonian perspective, with practical implementation and experimental validation. The report is organized as follows: Chapter 1 introduces the theoretical foundations of dielectrophoresis and the Port-Hamiltonian modeling framework; Chapter 2 presents the results of simulation studies; and Chapter 3 describes the experimental setup, PCB design, and observed particle motion.

# Chapter 1

# Theoretical Background: Dielectrophoresis and Port-Hamiltonian Modeling

## 1.1 Introduction to Dielectrophoresis

Dielectrophoresis (DEP) is the phenomenon whereby a neutral but polarizable particle experiences a force when subjected to a non-uniform electric field. Unlike electrophoresis, DEP does not require a net charge on the particle; instead, it arises from the interaction of an induced dipole moment with spatial variations in the electric field.

This effect was first systematically described by Herbert A. Pohl in the 1950s and has since become an essential technique in microfluidics, biophysics, and lab-on-chip technologies. DEP can be applied to cells, colloids, beads, and dielectric microparticles, enabling separation, trapping, and transport without chemical labeling.

The general expression of the DEP force for a spherical particle is:

$$\mathbf{F}_{DEP} = 2\pi\varepsilon_m r^3 \,\mathrm{Re}\{K(\omega)\}\,\nabla|\mathbf{E}|^2 \tag{1.1}$$

where:

- $r$: radius of the spherical particle,
- $\varepsilon_m$: permittivity of the surrounding medium,
- $\mathbf{E}$: local electric field,
- $K(\omega)$: Clausius–Mossotti factor.

The Clausius–Mossotti factor is given by:

$$K(\omega) = \frac{\varepsilon_p^* - \varepsilon_m^*}{\varepsilon_p^* + 2\varepsilon_m^*} \tag{1.2}$$

with the complex permittivity:

$$\varepsilon^* = \varepsilon - \frac{j\sigma}{\omega} \tag{1.3}$$

where $\varepsilon$ is the permittivity, $\sigma$ the conductivity, and $\omega$ the angular frequency of the applied field.

- **Positive DEP (pDEP):** $\mathrm{Re}(K) > 0$, particle attracted to regions of high field intensity.
- **Negative DEP (nDEP):** $\mathrm{Re}(K) < 0$, particle repelled toward regions of low field intensity.

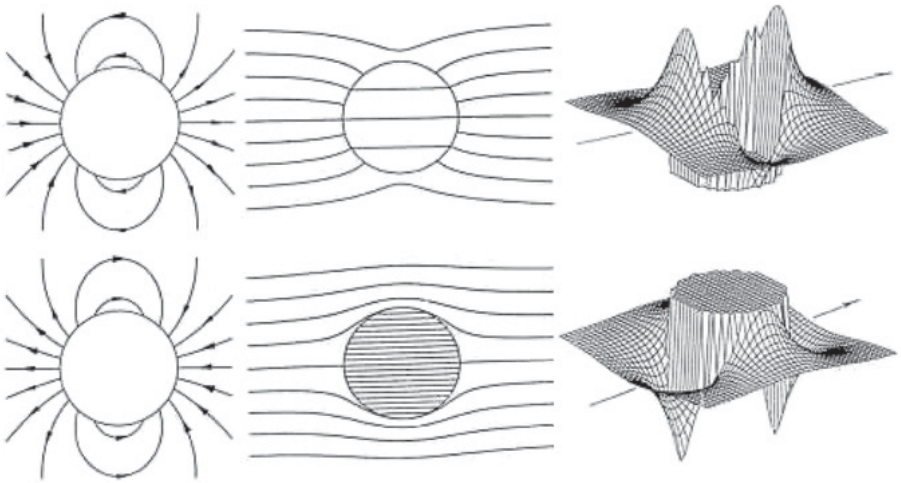

Figure 1.1: Schematic of positive (top row) and negative (bottom row) dielectrophoresis. Each row shows: **(left)** electric field lines around a polarized particle, **(center)** equipotential lines, and **(right)** a 3D map of field intensity. In positive DEP, the particle is attracted toward regions of higher electric field strength, while in negative DEP it is repelled toward regions of weaker field intensity [2].

## 1.2 Applications of Dielectrophoresis

DEP has numerous applications in micro- and nanotechnology:

- **Biomedical engineering:** cell sorting, cancer cell detection, bacteria trapping,
- **Microfluidics:** manipulation of particles in lab-on-chip devices,
- **Nanotechnology:** assembly of nanowires and nanotubes using electric fields.

## 1.3 Energy Perspective on DEP

Dielectrophoresis is essentially an energy-gradient phenomenon. The particle moves in response to variations in the electric energy density:

$$W_e = \frac{1}{2}\varepsilon|\mathbf{E}|^2 \tag{1.4}$$

The DEP force can be derived as the gradient of the interaction energy between the induced dipole and the field:

$$\mathbf{F}_{DEP} = \nabla\left(\mathbf{p}\cdot\mathbf{E}\right) \tag{1.5}$$

This energy-based perspective motivates the use of the Port-Hamiltonian formulation, which explicitly relies on power flow and energy conservation.

## 1.4 Port-Hamiltonian Systems: An Overview

Port-Hamiltonian (PH) systems provide a general mathematical framework to describe dynamical systems in terms of energy storage, dissipation, and interconnection. The generic PH system is expressed as:

$$\dot{x} = \left(J(x) - R(x)\right)\nabla H(x) + g(x)u, \qquad y = g^T(x)\nabla H(x) \tag{1.6}$$

where:

- $x$: state vector,
- $H(x)$: Hamiltonian (total stored energy),
- $J(x)$: skew-symmetric interconnection matrix (power-preserving),

- $R(x)$: positive semi-definite dissipation matrix,
- $u, y$: input and output ports.

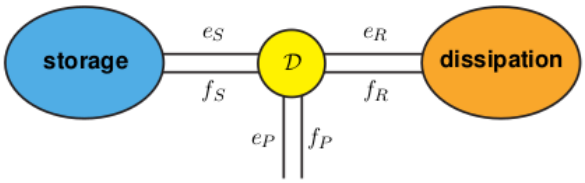


Figure 1.2: Block diagram representation of a Port-Hamiltonian system [2].

## 1.5 Port-Hamiltonian Formulation of DEP

In the DEP context:

- **States ($x$):** particle position $q$, momentum $p$, and induced polarization,
- **Hamiltonian ($H$):** sum of kinetic energy and electric energy of the induced dipole,

$$H = \frac{1}{2m}p^2 + \frac{1}{2}\alpha|E(q)|^2 \tag{1.7}$$

where $\alpha$ is the particle polarizability.

The Port-Hamiltonian formulation provides a unified model linking:

1. Applied electrode voltages,
2. Electric field distribution,
3. Induced dipole polarization,
4. Mechanical displacement of the particle.

$$H_p(\rho,\sigma) = \frac{1}{m}\rho^2 + \left(\frac{\rho_m}{\rho_p} - 1\right) gVy + C_{\mathrm{DEP}}\left|\vec{E}\right|^2$$

$$C_{\mathrm{DEP}} = 2\pi R^3 \varepsilon_m \,\mathrm{Re}(K_{\mathrm{CM}}), \quad \left|\vec{E}\right| = k_c \int_S \frac{\sigma}{d^2}\, dS, \quad k_c = \frac{1}{4\pi\varepsilon_m}$$

Figure 1.3: Conceptual diagram: DEP modeled within the Port-Hamiltonian framework [1].

## 1.6 Conclusion

This chapter introduced the fundamental principles of dielectrophoresis, its mathematical formulation, and its integration into the Port-Hamiltonian framework. While DEP describes how non-uniform electric fields induce forces on polarizable particles, the PH approach provides an elegant and systematic way to model the associated energy flows.

The following chapter builds upon these foundations with simulation studies of particle dynamics under DEP forces and electrode configurations.

# Chapter 2

# Numerical Studies and Simulation Results

## 2.1 Introduction

This chapter presents the numerical studies carried out during the internship to better understand the interaction between a dielectric particle and a non-uniform electric field. The central objective was to progressively develop a reliable model of dielectrophoresis (DEP), where particle motion results from induced polarization in the presence of a field gradient.

To achieve this, three complementary studies were conducted:

1. **Study 1** investigated the validity of the assumption of local uniformity of the electric field around a microparticle.
2. **Study 2** analyzed the electric potential and field inside and outside the particle, using both analytical and numerical methods.
3. **Study 3** validated the equivalent dipole approximation by comparing induced charges obtained from analytical derivations and numerical simulations under different electrode voltage configurations.

Finally, a **Python-based simulation model** was developed to consolidate these studies, serving as a bridge between theoretical models and the experimental phase presented in Chapter 3.

## 2.2 Study 1: Local Electric Field Uniformity

### 2.2.1 Objective

The first study aimed to determine whether the electric field in the vicinity of a dielectric microparticle could be considered locally uniform depending on the particle size. This is a crucial assumption, as it simplifies the mathematical treatment of dielectrophoresis while remaining valid for many microscale systems.

### 2.2.2 Methodology

- A spherical dielectric particle with diameters ranging from $2\,\mu$m to $7\,\mu$m was placed in a weakly non-uniform field.
- The *uniformity factor* $f(x)$ was introduced to quantify deviations of the field from uniformity.
- This factor was compared against a *dynamic threshold* $f_{\text{threshold}}$, derived from theoretical DEP conditions.

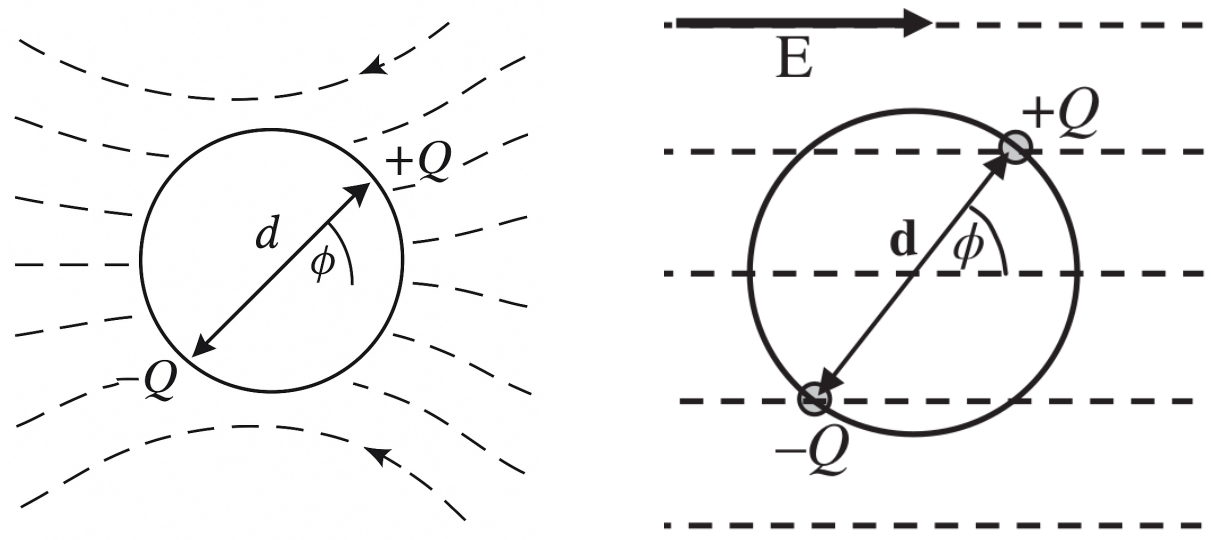


(a) Polarization of a particle in a uniform electric field.

(b) Polarization of a particle in a non-uniform electric field.

Figure 2.1: Comparison between particle polarization in uniform and non-uniform electric fields [2].

### 2.2.3 Results

The quantitative results of this analysis are illustrated in **Figure 2.2** (Figure 2.2), which highlights the relationship between particle size and the validity of the local uniform field assumption.

- For small particles ($\approx 2\,\mu$m), the deviations of the electric field remained negligible, confirming that the field can be locally approximated as uniform in the particle's vicinity.
- For larger particles ($\approx 7\,\mu$m), the deviations clearly exceeded the theoretical threshold, indicating that the quasi-uniform approximation becomes invalid in this regime.

The conclusion was that for particles below $6\,\mu$m in diameter, the dipole approximation remains accurate, while for larger particles higher-order multipole effects should be considered.

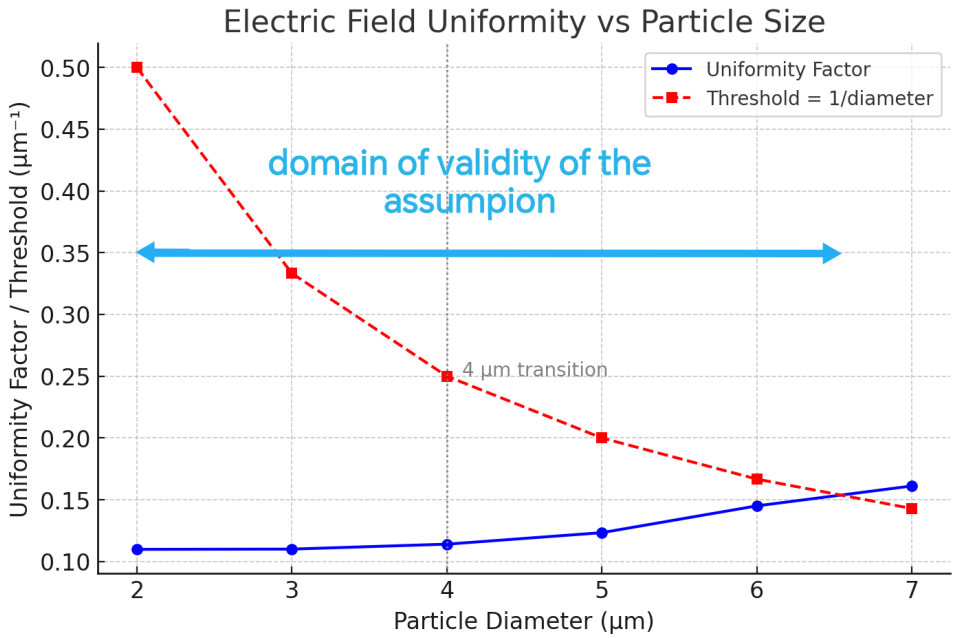


Figure 2.2: Evolution of the uniformity factor $f(x)$ as a function of particle size. The threshold $f_{\text{threshold}}$ indicates the validity limit of the local uniform field approximation.

## 2.3 Study 2: Evaluation of Electric Potential and Field

### 2.3.1 Objective

The second study focused on the evaluation of the electric potential and field both inside and outside the particle, using a dual approach:

- **Analytical derivations** based on Maxwell's equations and boundary conditions using a Python script,
- **Numerical simulations** using COMSOL Multiphysics.

### 2.3.2 Analytical Framework

- Inside the particle ($r < R$): the potential was derived by solving Laplace's equation, enforcing continuity of the electric displacement field across the particle boundary.
- Outside the particle ($r > R$): the particle was modeled as an induced dipole, leading to a potential of the form:

$$\Phi(r, \theta) = -E_0 r \cos\theta + \frac{p}{4\pi\varepsilon_m r^2} \cos\theta \tag{2.1}$$

where $E_0$ is the applied field, $p$ the dipole moment, and $\varepsilon_m$ the permittivity of the medium.
The Clausius–Mossotti factor was included to capture the contrast between particle and medium permittivity:

$$K(\omega) = \frac{\varepsilon_p^* - \varepsilon_m^*}{\varepsilon_p^* + 2\varepsilon_m^*} \tag{2.2}$$

### 2.3.3 Results

- Good agreement was observed between analytical and numerical results for the interior field and at the particle center.

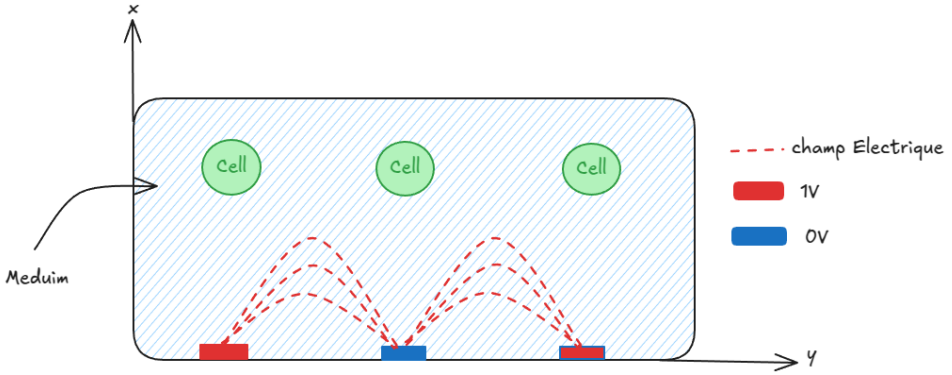


Figure 2.3: Schematic of Study 2: cells exposed to a non-uniform electric field created by alternating 1 V (red) and 0 V (blue) electrodes.

- At the particle boundary, small discrepancies appeared due to fringe effects that are more accurately captured by numerical solvers.

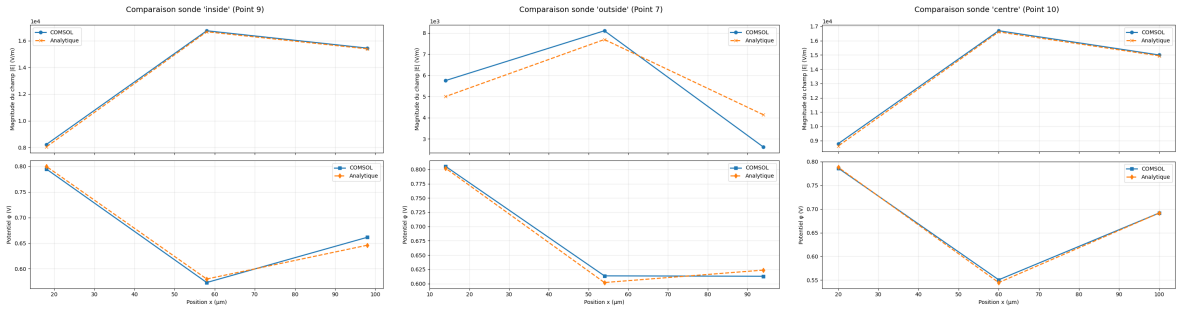


(a) Comparaison sonde *inside*. (b) Comparaison sonde *outside*. (c) Comparaison sonde *centre*.

Figure 2.4: Résultats de l'étude 2 : comparaison des champs électriques et potentiels simulés (COMSOL) et analytiques aux points sélectionnés.

## 2.4 Study 3: Validation of the Equivalent Dipole Model

### 2.4.1 Objective

The third study tested the validity of the equivalent dipole approximation by comparing the total induced charge predicted analytically with results obtained from numerical simulations.

### 2.4.2 Methodology

- The particle was modeled as a dielectric sphere of radius $R$ with complex permittivity $\varepsilon_p^*$, suspended in a medium of permittivity $\varepsilon_m^*$. The induced dipole moment $\mathbf{p}$ is given by:

$$\mathbf{p} = 4\pi\varepsilon_m R^3 K(\omega)\,\mathbf{E},$$

  where $K(\omega)$ is the Clausius–Mossotti factor:

$$K(\omega) = \frac{\varepsilon_p^* - \varepsilon_m^*}{\varepsilon_p^* + 2\varepsilon_m^*}.$$

- The induced dipole corresponds physically to a surface charge distribution $\sigma$ such that:

$$\sigma(\theta) = \varepsilon_0 E \cos(\theta)\, K(\omega),$$

where $\theta$ is the angle relative to the applied field direction.

- The dielectrophoretic (DEP) force acting on the particle is expressed as:

$$\mathbf{F}_{DEP} = \frac{1}{2}\,\mathrm{Re}\big[\,\alpha(\omega)\,\nabla|\mathbf{E}|^2\,\big]\,,$$

with polarizability $\alpha(\omega) = 4\pi\varepsilon_m R^3 K(\omega)$.

- The electric field was obtained from the potential $\phi$ by:

$$\mathbf{E} = -\nabla\phi.$$

- Different electrode voltage configurations were applied in COMSOL and in the analytical model, including:

$$(1,0,1)\,\mathrm{V}, \quad (2,0,2)\,\mathrm{V}, \quad (0,1,1)\,\mathrm{V}, \quad (1,5,3)\,\mathrm{V}.$$

- For validation, the induced charges $Q$ were computed both numerically (COMSOL surface integration) and analytically (from dipole approximation):

$$Q = \int_S \sigma\, dS \quad \text{and} \quad Q_{\text{ana}} = |\mathbf{p}|/R.$$

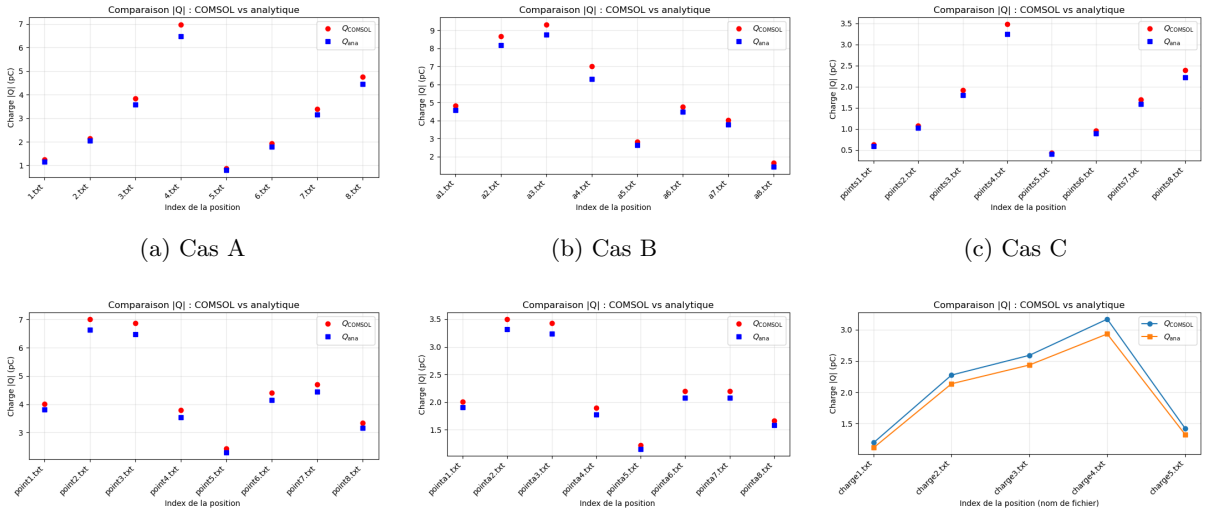


(a) Cas A (b) Cas B (c) Cas C

(d) Cas D (e) Cas E (f) Cas F

Figure 2.5: Comparaison compacte de la charge $|Q|$ : COMSOL (rouge) vs analytique (bleu) pour différents points de mesure.

## 2.5 Simulation Model Development

To consolidate the insights from the three studies, a Python-based simulation framework was developed (see Appendix for code). The workflow follows the energy–charge–force chain, illustrated in Fig. 2.6a, where the induced surface charge density drives the electric field distribution, which in turn defines the equivalent charge and dielectrophoretic (DEP) force.

### 2.5.1 Model Features

- **Inputs:** particle radius $R$, medium permittivity $\varepsilon_m$, electrode geometry and applied voltages $V_i$.
- **Core calculations:**

– Electric field from surface charge distribution:

$$|\vec{E}| = k_c \int_S \frac{\sigma}{d^2}\, dS, \quad k_c = \frac{1}{4\pi\varepsilon_m},$$

– Equivalent induced charge:

$$Q = \pi\varepsilon_m R K E_0,$$

– DEP force:

$$F_{DEP} = Q\, 2R\, \frac{\partial E}{\partial r} = (\vec{p}\cdot\nabla)\vec{E},$$

– Full dipole-based expression (time-averaged DEP force):

$$\vec{F}_{DEP} = 2\pi\varepsilon_m R^3\, \mathrm{Re}[K(\omega)]\, \nabla|\vec{E}|^2.$$

### 2.5.2 Outputs

- Electric field and potential maps,
- Equivalent charge distribution on electrodes,
- DEP force quadrant indicators (Fig. 2.6b),
- Estimated particle trajectories under different voltage configurations.

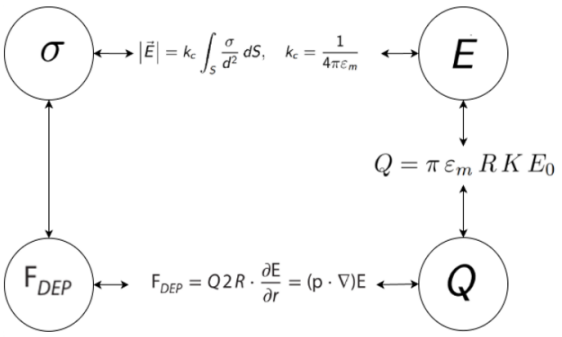


(a) Workflow of the simulation model: $\sigma \to \vec{E} \to Q \to F_{DEP}$.

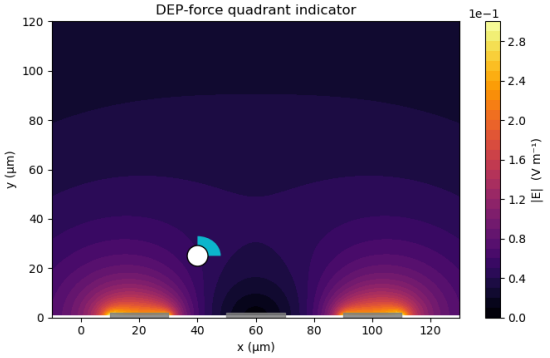


(b) DEP force quadrant indicator at $(40\,\mu\mathrm{m}, 25\,\mu\mathrm{m})$ for $(1, 0, 1)$ V.

Figure 2.6: Simulation model and output results.

## 2.6 Conclusion

Through these three studies and the development of a simulation model, the theoretical basis of dielectrophoresis was rigorously analyzed. The results confirmed the applicability of the dipole approximation at the microscale, the robustness of the analytical–numerical comparison, and the feasibility of predicting particle motion in controlled non-uniform fields.

This chapter lays the foundation for the experimental work presented in the following section, where the theoretical insights are confronted with real-world observations using fabricated PCB electrodes and oscilloscope measurements.

# Chapter 3

# Hardware Development and Experimental Validation

This chapter details the hardware development and the experimental validation process carried out during the internship. The goal was to design, assemble, and test a dedicated printed circuit board (PCB) capable of delivering controlled sinusoidal voltages to several electrodes, in order to reproduce non-uniform electric fields for dielectrophoresis (DEP) experiments. Beyond the PCB design and assembly, bench tests were conducted to ensure the reliability of the signals, followed by a laboratory experiment to observe the actual motion of microparticles under DEP forces.

## 3.1 PCB Design and Objectives

The PCB represents the core interface between the theoretical models, simulations, and experimental validation. Its primary role is to generate multiple sinusoidal voltages with precise amplitudes and phases and deliver them to electrode pairs, enabling the creation of tunable non-uniform electric fields.

In dielectrophoresis, the induced force on a particle is proportional to the gradient of the squared electric field. This makes it essential to design a system capable of dynamically applying voltages that not only reproduce simple analytical conditions but also allow flexible electrode excitation, as required in the simulation studies. In practice, this means generating sinusoidal signals whose amplitudes scale with the applied input, ensuring that electrode configurations can replicate both theoretical and COMSOL-based study conditions.

### 3.1.1 Architecture of a Single Channel

Each PCB channel is based on a modular architecture (Fig. 3.1):

- **Input stage:** An analog multiplier (AD734) is used to combine two input signals. One input is a rectangular voltage that mimics a DC reference, while the other is a sinusoidal signal. The result is a sinusoidal output whose amplitude follows the DC reference level, making it possible to scale voltages dynamically.
- **Buffer and amplification:** A precision operational amplifier (OP42) buffers the multiplied signal, stabilizes it, and ensures low distortion even at high frequency.
- **Output stage:** The final signal is routed to SMA connectors, chosen for their excellent impedance matching and low-loss transmission.

### 3.1.2 Full Schematic and Layout

The complete PCB consists of several identical channels, each independently powered and addressable. This modularity allows multiple electrodes to be excited simultaneously with different amplitudes and phases.

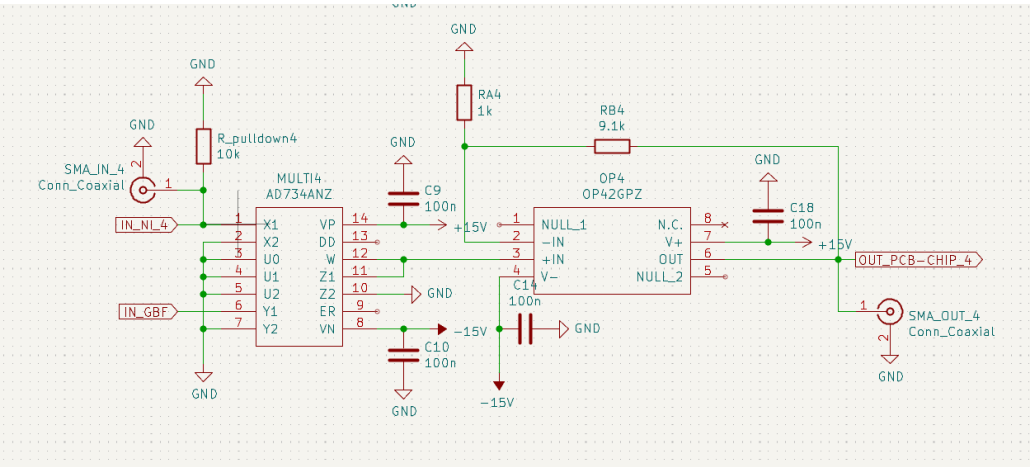


Figure 3.1: Schematic of a single PCB channel with analog multiplier (AD734) and buffer amplifier (OP42).

Figure 3.2 shows the full schematic of the PCB, where each block corresponds to one channel. Local decoupling capacitors and resistors were added to reduce coupling noise and improve stability.

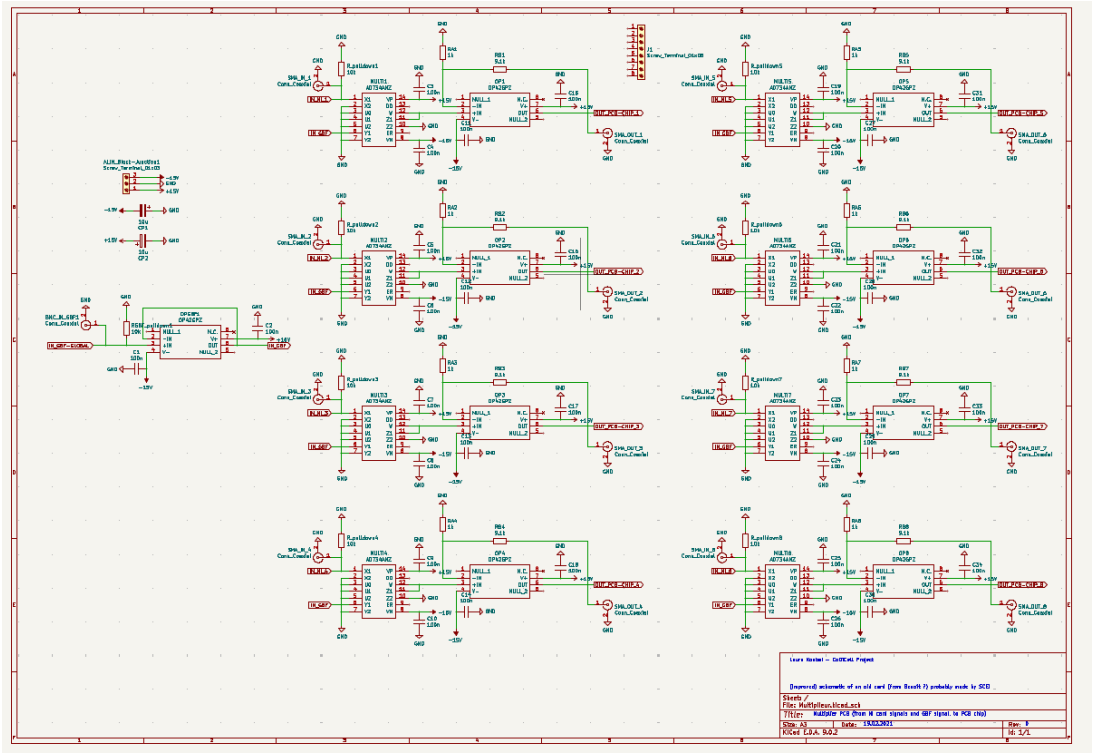

Figure 3.2: Complete schematic of the PCB with replicated channels for multiple electrode excitation.

A central **junction block** was also included to distribute common supply rails (+15 V, −15 V, GND) and shared control signals to all channels. This distribution node reduces wiring complexity and ensures stable powering of the multipliers and amplifiers. By soldering this block, the inputs and outputs could be routed cleanly, facilitating quick experimental reconfigurations.

The PCB layout is shown in Fig. 3.3, with SMA connectors clearly arranged for straightforward cabling. The compact and symmetric design ensures low parasitic coupling between channels.

Finally, the fabricated bare PCB before assembly is presented in Fig. 3.4.

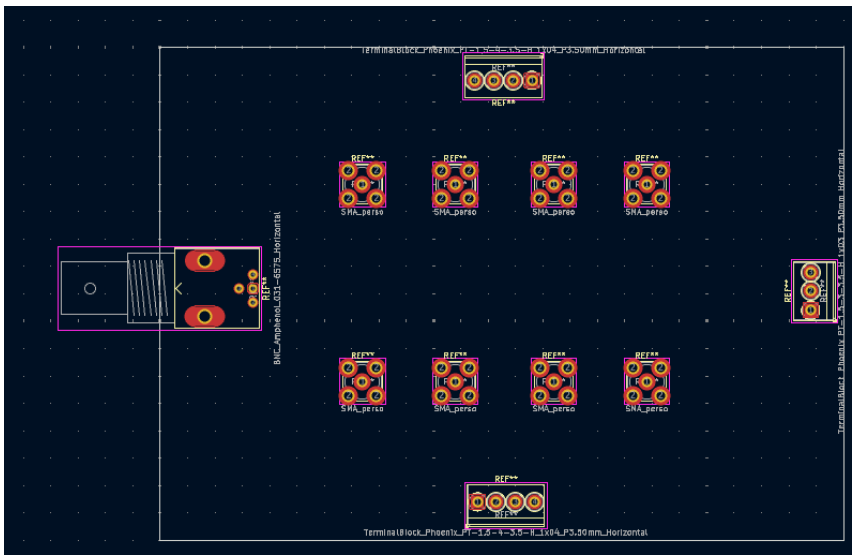


Figure 3.3: PCB layout with SMA connectors and footprints for multipliers and amplifiers.

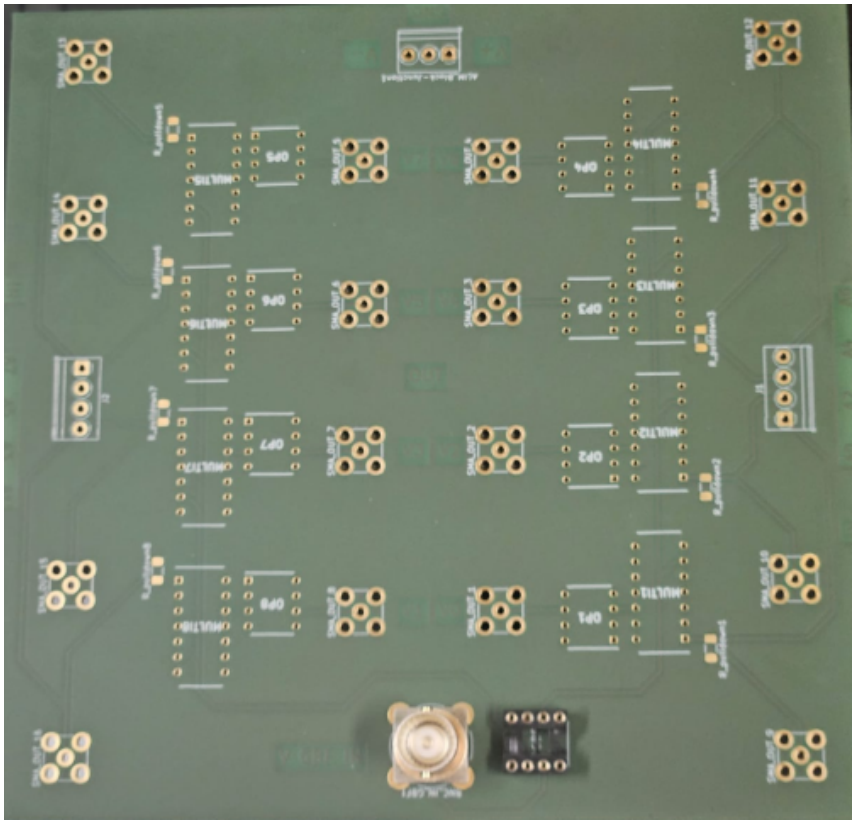

Figure 3.4: Manufactured PCB before soldering.

## 3.2 Assembly and Bench Testing

### 3.2.1 Soldering Process

The PCB was soldered manually using a stereo microscope to ensure precise component placement. Special care was taken with the analog multipliers (AD734) and operational amplifiers (OP42), since their correct soldering and decoupling directly affect the signal integrity. The junction and SMA inputs/outputs were also soldered to guarantee robust connections for experimental use.

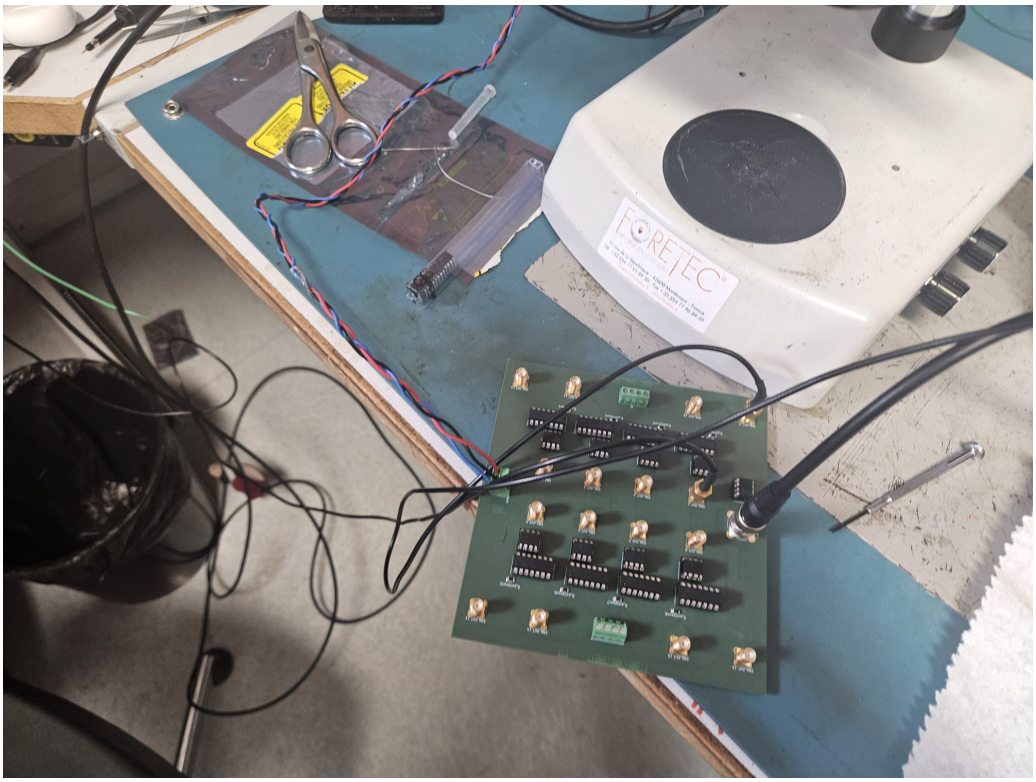


Figure 3.5: PCB during soldering and visual inspection under the microscope.

### 3.2.2 Test Configuration

To validate the system, two signals were applied to each multiplier:

- A rectangular signal acting as a **DC reference**.
- A sinusoidal signal at the desired frequency.

The multiplier output therefore produced a sinusoidal waveform whose amplitude was directly proportional to the reference voltage. For example, when the DC reference was 10 V, the sinusoidal output had an amplitude of 10 V as well.

Figure 3.6 shows the laboratory signal source used to generate the two inputs.

This principle was validated experimentally on the oscilloscope, as illustrated in Fig. 3.7, where the expected sinusoidal output was observed.


Figure 3.6: Signal source used for generating the rectangular (DC reference) and sinusoidal inputs.

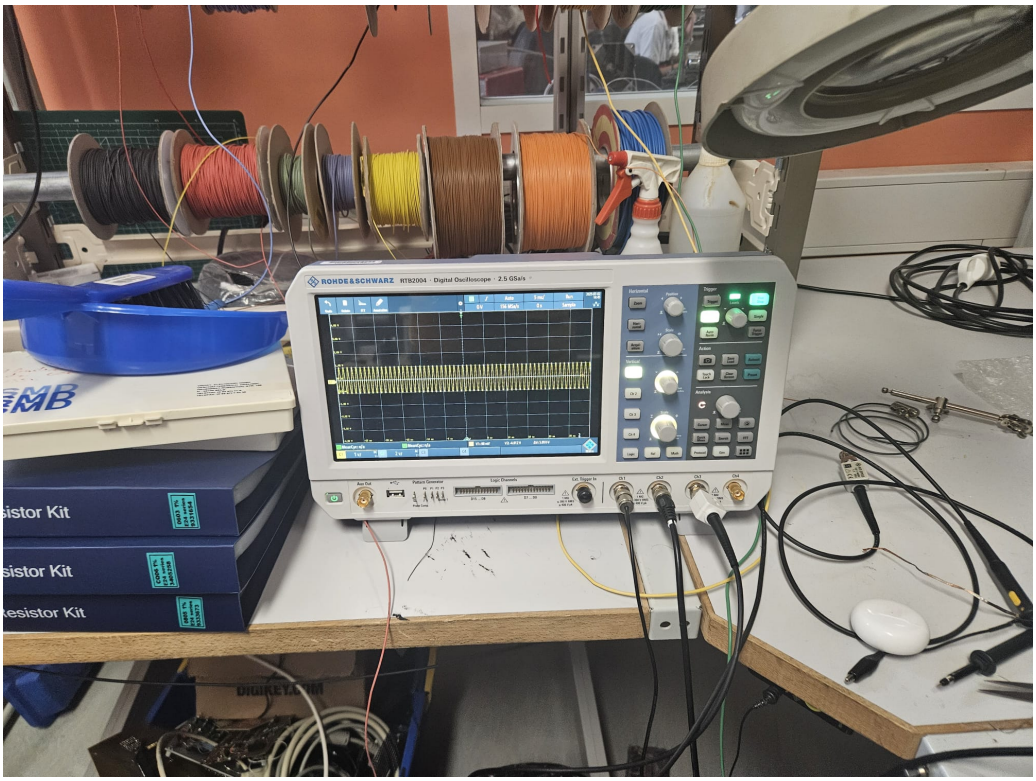


Figure 3.7: Oscilloscope output: sinusoidal signal with amplitude scaling by DC reference input.

## 3.3 Real DEP Experiment

After validating the PCB through bench testing, the final phase of this internship consisted of conducting real dielectrophoresis (DEP) experiments to observe and analyze the motion of dielectric microparticles under non-uniform electric fields. This section presents the experimental setup, detailed protocols, and observed results for two configurations:

- the **dynamic flow experiment**, where particles are carried by a fluid flow and steered laterally by DEP forces,
- the **static suspension experiment**, where particles are suspended without flow and migrate due solely to DEP.

### 3.3.1 Materials and Setup

**Particles and medium.** Experiments used dielectric microparticles (silica or polystyrene) with diameters starting from $20\,\mu$m, suspended in deionized water with low conductivity ($\sigma_m \approx 10^{-3}\,\mathrm{S/m}$). The low-conductivity medium minimizes electrochemical reactions and ensures that polarization effects dominate particle motion.

**Electrode configuration.** The electrodes were fabricated on a custom PCB designed in this work. Each electrode was driven by an independent sinusoidal voltage from the analog multiplier and amplifier circuit described in Sec. 3.1. SMA connectors ensured low-loss transmission and phase stability across the three output channels.

**Signal generation.** The PCB generated sinusoidal voltages with adjustable amplitudes and frequencies (as used in Chapter 2). These signals reproduced electrode configurations such as $(1, 0, 1)\,\mathrm{V}$, $(2, 0, 2)\,\mathrm{V}$, and $(1, 5, 3)\,\mathrm{V}$.

**Observation system.** A high-magnification optical microscope equipped with a digital camera (60 fps) was used to record particle motion in real time. All videos were captured under constant lighting and magnification for later quantitative analysis.

### 3.3.2 Dynamic Flow Experiment

**Objective.** To demonstrate active lateral steering of microparticles flowing through a microchannel using non-uniform electric fields.

**Procedure.** A dilute suspension of microparticles was injected through a straight microchannel positioned over the electrodes. The PCB applied a voltage configuration that generated a lateral field gradient. Depending on the sign of the Clausius–Mossotti factor $\mathrm{Re}\{K(\omega)\}$, particles were either attracted ($pDEP$) or repelled ($nDEP$) from the high-field region. Videos were recorded for each pattern.

**Results and observations.** Particles were clearly deflected toward one side of the channel when a non-symmetric voltage pattern was applied. Reversing the voltage configuration reversed the steering direction, confirming that the observed drift was produced by DEP forces rather than hydrodynamic effects. The measured lateral deviation increased with voltage amplitude.

### 3.3.3 Static Suspension Experiment

**Objective.** To observe dielectrophoretic migration and trapping of particles in a quiescent fluid, without the influence of hydrodynamic flow.

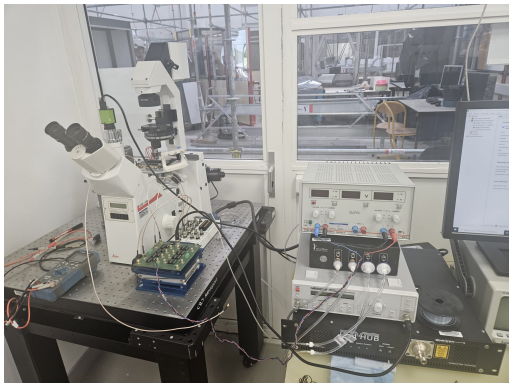

(a) Experimental setup: microscope observation of the flow channel driven by the PCB.

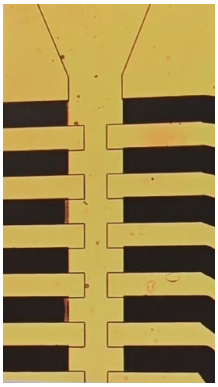

(b) Result: lateral steering of microparticles under non-uniform electric fields.

Figure 3.8: Dynamic flow DEP experiment: (a) setup and (b) observed steering of particles.

**Procedure.** A droplet of microparticle suspension was deposited directly on the electrode area. Once the particles settled, sinusoidal voltages were applied with different electrode configurations. Depending on the applied pattern, particles either accumulated near the high-field region (positive DEP) or were expelled (negative DEP). Each experiment lasted approximately one minute, and videos were analyzed using frame-by-frame tracking.

**Results and observations.** Initially, the particles naturally gathered near the center of the electrode region, forming dense clusters due to local field gradients. When different voltage configurations were applied, the balance of forces shifted and the clusters gradually dispersed, causing the particles to move collectively in a single, well-defined direction. This directional motion reflected the reorientation of the electric field lines and demonstrated the ability to control particle migration dynamically through dielectrophoretic actuation. The observed behavior was consistent with the field distribution predicted by the simulations, confirming the accuracy of both the model and the PCB-generated signals.

(a) Experimental setup: static suspension with microscope view over the electrodes.

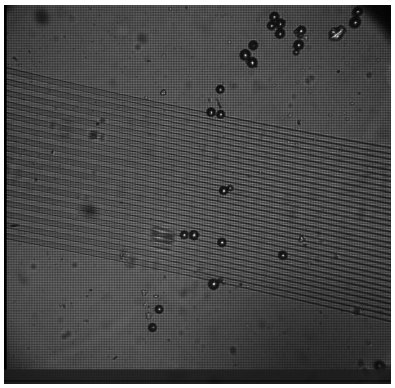

(b) Result: particle migration and trapping due to DEP forces (see video https://youtube.com/shorts/7AtHHy21Yko).

Figure 3.9: Static DEP experiment: (a) setup and (b) observed motion of particles under different voltage configurations.

### 3.3.4 Discussion and Analysis

The two experiments confirm the theoretical predictions made in Chapter 2:

- The sign of $\mathrm{Re}\{K(\omega)\}$ determines whether particles are attracted (pDEP) or repelled (nDEP) from high-field zones.
- The experimental steering directions and relative intensities between configurations match the simulated results.

Overall, the PCB platform provided reliable and tunable excitation signals, and the observed results strongly validate the port-Hamiltonian DEP model developed earlier in this work.

# Conclusion and Perspectives

This internship at FEMTO-ST (AS2M) provided a complete path from modeling to practice in microrobotics. The work (i) consolidated DEP theory with an energy-consistent viewpoint, (ii) validated analytical predictions against numerical simulations across electrode patterns, (iii) produced a robust multi-channel PCB capable of amplitude-scaled sinusoidal outputs, and (iv) demonstrated DEP-based manipulation in both dynamic and static conditions.

The experience strengthened my research skills—posing precise questions, building and comparing models, designing validation protocols, and iterating between theory and experiment. Going forward, promising directions include frequency sweeps to map $\mathrm{Re}\{K(\omega)\}$ transitions, port–Hamiltonian feedback control for trapping/sorting, exploration of electrode geometries for stronger gradients, quantitative trajectory tracking for parameter identification, and tighter integration of PCB, microfluidics, and optics into a compact DEP platform.

# Bibliography

[1] Nelson Cisneros, Yongxin Wu, Kanty Rabenorosoa, and Yann Le Gorrec. Port-hamiltonian modeling and control of a curling hasel actuator. *IFAC-PapersOnLine*, 58(6):143–148, 2024.

[2] Ronald R Pethig. *Dielectrophoresis: Theory, methodology and biological applications*. John Wiley & Sons, 2017.